Research Article Vol. 57, No. 21 / 20 July 2018 / Applied Optics 6233

applied optics

# Simulated annealing optimization in wavefront shaping controlled transmission

Zahra Fayyaz,[1] Nafiseh Mohammadian,[2,3] Faraneh Salimi,[2,4] Afreen Fatima,[2] M. Reza Rahimi Tabar,[1] and Mohammad R. N. Avanaki[2,5,6,*]

[1]Department of Physics, Sharif University of Technology, Tehran 11365-9161, Iran
[2]Biomedical Engineering Department and School of Medicine, Wayne State University, Detroit, Michigan 48201, USA
[3]CREOL, The College of Optics and Photonics, University of Central Florida, Orlando, Florida 32816, USA
[4]Industrial Engineering Department, Wayne State University, Detroit, Michigan 48201, USA
[5]Department of Dermatology, School of Medicine, Wayne State University, Detroit, Michigan 48201, USA
[6]Barbara Ann Karmanos Cancer Institute, Detroit, Michigan 48201, USA
*Corresponding author: mrn.avanaki@wayne.edu

Received 17 May 2018; revised 17 May 2018; accepted 24 May 2018; posted 22 June 2018 (Doc. ID 319134); published 20 July 2018

**In this research, we present results of simulated annealing (SA), a heuristic optimization algorithm, for focusing light through a turbid medium. Performance of the algorithm on phase and amplitude modulations has been evaluated. A number of tips to tune the optimization parameters are provided. The effect of measurement noise on the performance of the SA algorithm is explored. Additionally, SA performance is compared with continuous sequential and briefly with other optimization algorithms.** 

***OCIS codes:*** (030.6600) Statistical optics; (100.3200) Inverse scattering; (130.4110) Modulators; (290.1990) Diffusion; (290.4210) Multiple scattering; (290.7050) Turbid media.

https://doi.org/10.1364/AO.57.006233

## 1. INTRODUCTION

Smart control of light propagation through a highly scattering medium has been a much-desired goal with applications such as deep-tissue imaging, optical encryption, and quantum information processing [1]. Such control has been achieved by optimizing the shape of the wavefront of the incident light using spatial light modulators (SLMs) or digital micromirror devices (DMDs), and a feedback system; this technique is known as wavefront shaping [2,3]. Wavefront shaping techniques enhance the signal-to-noise ratio and imaging depth in optical imaging systems, e.g., optical coherence tomography [4–6], fluorescence microscopy [7], two-photon microscopy [8–10], multiphoton microscopy [11], photo-acoustic microscopy [12–14], etc., when a highly scattering medium is imaged. Wavefront shaping has also been used for photodynamic therapy, photostimulation of cells/tissues, and multimode optical fiber-based endoscopy [15]. Moreover, wavefront shaping has been applied to many other applications, including control of the spatiotemporal characteristics of random lasers [16–19], achievement of spectral control of a broadband light source [20–23], compression of ultrashort pulses [24,25], control of polarization [26,27], achievement of perfect focusing [28,29], phase conjugation of fluorescence in turbid tissue [30], tunable beam splitters [31], spatial control of second-harmonic light [32,33], control of single-photon Fock-state propagation [34], control of photocurrent in disordered photovoltaics [35], focusing through dynamic tissue [36], improvement of free-space optical communication [37], image projection through disordered media [38], three-dimensional microscopy [39], creation of an ultrafast nanophotonic switch [40], and optical control of excitation waves in cardiac tissue [41,42]. In addition to this wide range of applications, controlled reflection has promising applications for optical authentication of optical physical unclonable functions [43,44].

Light scattering is the major obstacle in focusing light through biological tissues. Scattering in a tissue scrambles the incident photons in a highly disordered manner, especially after a few mean free paths [1]. Freund first proposed in 1990 that wavefront shaping could be used to focus light through an opaque medium [45]. Vellekoop and Mosk demonstrated this method, for the first time, in 2007 [2]. They experimentally showed that coherent light can be focused through a diffusive medium when an SLM is used. For any given medium, there is a unique wavefront shape that can compensate for the effects of scattering in the sample. This wavefront couples to the medium's transmission eigenchannels, which leads to an optimal transmission of light into a target channel.

Although light propagation through a diffusive medium seems unpredictable, it is a deterministic process, which follows Maxwell equations [15]. Light transport in a complex medium is considered a linear process, which can be described using a

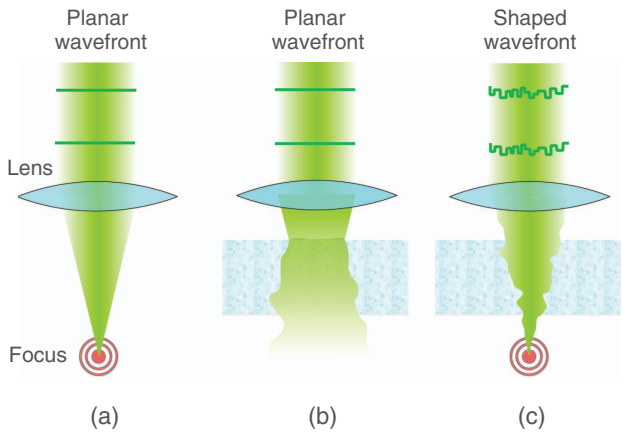


**Fig. 1.** Demonstration of light propagation through a turbid medium with and without wavefront shaping. (a) Light focusing with a lens in the absence of a turbid medium. (b) Light divergence due to multiple scattering. (c) Focusing through a turbid medium after wavefront shaping.

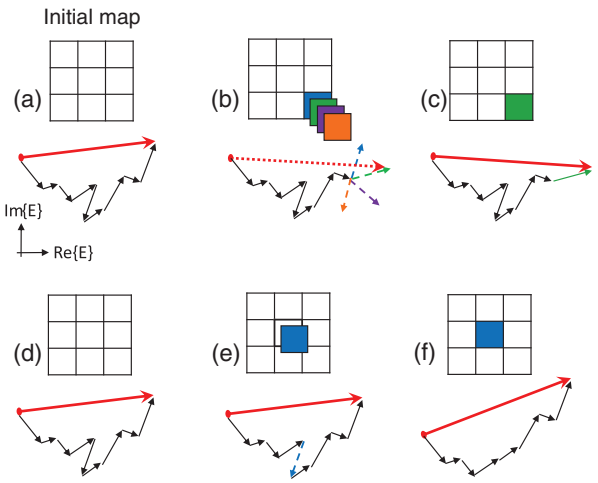


**Fig. 2.** (a)–(c) Graphical representation of phase modulation and (d)–(f) amplitude modulation. The small vectors show the electric field transmitted from each input channel. The red vector is the total electric field at the target output channel. In phase optimization, at each iteration, a segment is selected and the phase of the segment is varied. The blue, green, purple, and orange vectors represent the electric field at the target channel corresponding to four different phases. In amplitude optimization, at each iteration, a segment is turned on (white) or off (blue).

transmission matrix. This matrix describes how each segment of the incident light contributes to the constructive or destructive interference at each segment of the output speckle pattern [46]. By optimizing the impinging wavefront, i.e., spatially manipulating the wavefront phase, constructive interference at a desired target can be achieved (see Fig. 1).

While SLMs are usually used for phase modulation, DMDs are used for amplitude modulation. Although phase optimization provides a better focus in a turbid medium, DMDs are much faster. DMDs have refresh rates ≥kHz, whereas SLMs are demonstrated to have up to 180 Hz refresh rate (Meadowlark Optics now makes an SLM that can reach rates of up to 667 Hz) [3,43,47].

Several algorithms have been proposed for the optimization of a wavefront shaping system. The basic principle of all these algorithms involves dividing the wavefront into segments, i.e., the input channels, and then modulating each of these channels until a sharp focus is achieved.

In this study, we evaluate the simulated annealing (SA) algorithm for wavefront shaping to optimize phase in an SLM as well as amplitude optimization in a DMD. Measurement noise is a random error in the measurement of light intensity at the target channel. The effect of measurement noise on the performance of the SA algorithm for both SLM and DMD is also explored. All the results are compared with the continuous sequential (CS) algorithm, which is the classical algorithm for this purpose. However, several other algorithms have as well been proposed in recent years. We will provide a brief comparison with four other algorithms, namely, partitioning algorithm (PA) [2], transmission matrix (TM) [46] estimation method, particle swarm optimization (PSO) [48], and genetic algorithm (GA) [49].

## 2. MATERIALS AND METHODS

### A. Wavefront Optimization

In wavefront optimization, the phases or amplitudes of the input channels are modulated repetitively until a sharp focus is obtained. The linear relationship between the incident electric field and the electric field transmitted through a scattering medium can be described by a TM [see Eq. (1)]:

$$E_m = \sum_n^N t_{mn} E_n = \sum_n^N t_{mn} A_n e^{i\phi_n}, \quad (1)$$

where $E_m$ is the electric field at the $m$th output channel, $E_n$ is the electric field at the $n$th input channel, and $t_{mn}$ is an element of the TM. In our simulations, the incident light beam is illuminated on $N$ segments of a light modulator. Each segment is modulated with a specific phase, $\phi_n$, or an amplitude, $A_n$, in the case of phase or amplitude optimization, respectively. In order to maximize the strength of the focus, a single output channel is targeted.

The working principle of the phase and amplitude wavefront optimizations is demonstrated in Fig. 2. In this figure, a vectorial representation of the electric field in the selected target channel, $E_m$, is depicted. This electric field is a vectorial sum of the electric fields of all input channels multiplied by their corresponding elements of the TM. The top panels [Figs. 2(a)–2(c)] illustrate how phase modulation increases the strength of the focus, whereas the bottom panels [Figs. 2(d)–2(f)] illustrate the effect of amplitude modulation.

### B. SA Optimization Algorithm

SA is a heuristic optimization algorithm that is used to find the global optimum in a large search space. It is a numerical optimization technique based on the principles of thermodynamics suggested in 1953 by Metropolis *et al.* [50]. The algorithm simulates the cooling of a metal in a heat bath. This is a process known as annealing. If a solid is heated past its melting point and then cooled, the structural properties of the solid will depend on the rate of cooling. If the liquid is cooled slowly enough, large pure crystals will be formed with the minimum

energy. If, however, the liquid is cooled quickly (quenched), imperfect crystals will be formed. The SA algorithm simulates the cooling process by gradually lowering the temperature of the system until it converges to a steady state.

The concept of optimization using SA is depicted in Fig. 3. This cartoon demonstrates how to find the global minimum in a solution space with various local minima using SA. Temperature is a parameter that mimics the effect of a fast-moving particle in a hot molten metal. The SA algorithm begins the optimization at a high temperature. In Fig. 3, this is demonstrated by permitting the ball to jump over any mountain and potentially access the deepest valley if sufficient time is given or a sufficient number of iterations is allowed. As the temperature drops, the ball bounces much less and less favorable answers are not likely to be accepted.

The SA algorithm has previously been used for the optimization of optical systems [51–57]. In our study, we optimized a phase or an amplitude modulator using the SA algorithm until the strongest focus on a charge-coupled device (CCD) is achieved.

**Algorithm 1:** SA algorithm pseudocode. TM represents the transmission matrix, $T$ represents the temperature in the SA algorithm, and $T_0$ is the initial temperature. $\phi_1$ and $B_1$ are, respectively, the initial phase map and binary amplitude map (randomly generated). The text in red indicates changes in the pseudocode related to amplitude optimization.

```
TM ← Turbid medium transmission matrix
        with a Gaussian distribution
T ← T_0
φ_1 ← Random phase map
B_1 ← Random binary amplitude map
E_1 ← Initial intensity of focus
while Termination criteria are not met (i.e., T > T_min) do
  for L = 1 to L = loop length do          ▷ Perturbation loop
    φ_2 ← φ_1 + Phase perturbation
    B_2 ← Toggle(B_1)
    E_2 ← E(φ_2)                           ▷ Update focus intensity
    if E_2 > E_1 then
      φ_1 ← φ_2
      B_1 ← B_2
      E_1 = E_2                            ▷ Perturbed state is accepted
    else                                   ▷ Boltzmann condition
      if exp((E_2−E_1)/T) > rand(0, 1) then
        φ_1 ← φ_2
        B_1 ← B_2
        E_1 = E_2                          ▷ Perturbed state is accepted
  T = αT                                   ▷ Decrease temperature
```

The pseudocode of the SA algorithm is given in Algorithm 1. In this algorithm, a random TM with a circular Gaussian distribution, representing a scattering medium, is generated. An initial random phase map is also generated with values between 0 and $2\pi$ (SLM phase map). The strength of the focus point on the CCD, $E_0$, is calculated. A coarse perturbation is applied to the phases of the SLM segments, and the energy of the new system, with the new phase map, is calculated. If the energy is larger than the previous one, i.e., if the new focus is stronger, then the new perturbation will be accepted as the new state of the system. Otherwise, the perturbation has a lower chance of being accepted with the probability calculated in Boltzmann probability function [i.e., $\exp(\frac{E_2-E_1}{T})$] and is discarded. After going through a perturbation loop (i.e., applying $L$ coarse perturbations), the temperature drops by a factor of $\alpha$. After a certain number of perturbation loops, the perturbation size decreases; these are the fine perturbations, which will be executed until the end of run. In the amplitude optimization, the SA algorithm is utilized in a similar manner. In the algorithm, instead of a phase map, a binary amplitude map is used. Those parts of the pseudocode that are changed from phase modulation to amplitude modulation are shown in red in Algorithm 1.

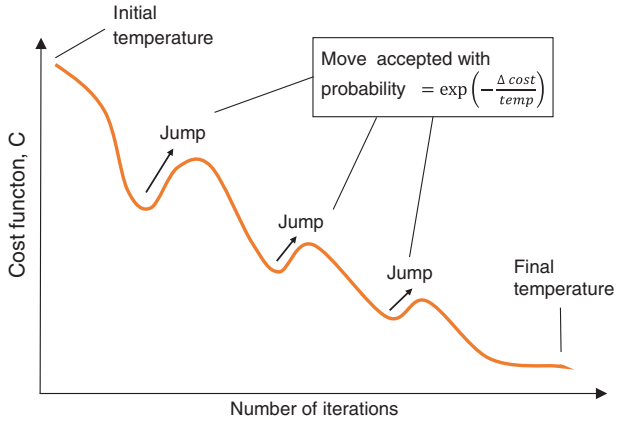


**Fig. 3.** Demonstration of SA optimization to find the global minimum in a minimization problem.

### C. Theory of Wavefront Shaping

In the phase optimization algorithm, we assume that the incident light homogeneously illuminates the modulator and all input channels carry the same intensity. We assume that the amplitude of each segment is $A_n = \frac{1}{\sqrt{N}}$. Elements $E_1, E_2, \ldots E_N$ correspond to the output channels. The goal is to focus the light on a single spot, i.e., strengthen a single output channel ($E_m$). The intensity transmitted into the output channel ($I_m$) is given by Eq. (2):

$$I_m = |E_m|^2 = \frac{1}{N}\left|\sum_n^N t_{mn} e^{i\phi_n}\right|^2. \tag{2}$$

Regardless of the values in the TM ($t_{mn}$), the intensity $I_m$ will have the maximum value when the phase modulator correctly compensates for the sample phase retardation in each segment, i.e., $\phi_n = -\arg(t_{mn})$. The intensities before optimization ($I_0$) and after an ideal optimization ($I_{\max}$) are given, respectively, by Eqs. (3) and (4):

$$I_0 = \frac{1}{N}\left|\sum_n^N t_{mn}\right|^2, \tag{3}$$

$$I_{\max} = \left(\sum_n^N |t_{mn}|\right)^2. \tag{4}$$

Assuming the elements of the TM are uncorrelated and follow a circular Gaussian distribution [58–61], Eq. (4) can be rewritten as

$$\langle I_{\max}\rangle = \left\langle \frac{1}{N}\sum_{n,k\neq m}^{N} |t_{mn}||t_{mk}| + \frac{1}{N}\sum_{n}^{N} |t_{mn}|^2 \right\rangle$$
$$= \langle I_0\rangle \left[\frac{(N-1)\pi}{4} + 1\right], \quad (5)$$

where the angled brackets denote ensemble averaging. Enhancement is defined as the ratio of the optimized focus intensity to the ensemble averaged intensity before optimization. Equation (5) predicts that the expected maximum enhancement ($\eta$) depends on the system size, i.e., the number of segments ($N$) in a stable and noise-free system. In phase optimization, for $N \gg 1$, $\eta \approx \pi\frac{N}{4}$. In amplitude optimization, if noise and instabilities are ignored, then the ensemble averaged intensity enhancement at the target position, $\eta_{\text{ideal}}$, is obtained as [3]

$$\eta_{\text{ideal}} = \frac{\langle I_{\max}\rangle}{\langle I_0\rangle} = 1 + \frac{1}{\pi}\left(\frac{N}{2} - 1\right) \approx \frac{N}{2\pi}. \quad (6)$$

### D. Simulation

The simulation setup is shown in Fig. 4. In this simulation, a wavefront shaping system including a CCD and a phase/amplitude modulator (an SLM or a DMD) were used. The modulated field is then projected onto a turbid medium. The pattern of the outgoing light field is measured by the CCD. A modified phase/amplitude map is then sent to the modulator to create a sharp focus.

### E. Parameter Setting

There are several parameters in the SA algorithm to be determined. There is no standard method to fine-tune these parameters. We provide a number of tips to determine these parameters such that an optimum solution is obtained. The impact of the parameters on the performance of SA is also evaluated. We used two measures for evaluation, namely, runtime and enhancement.

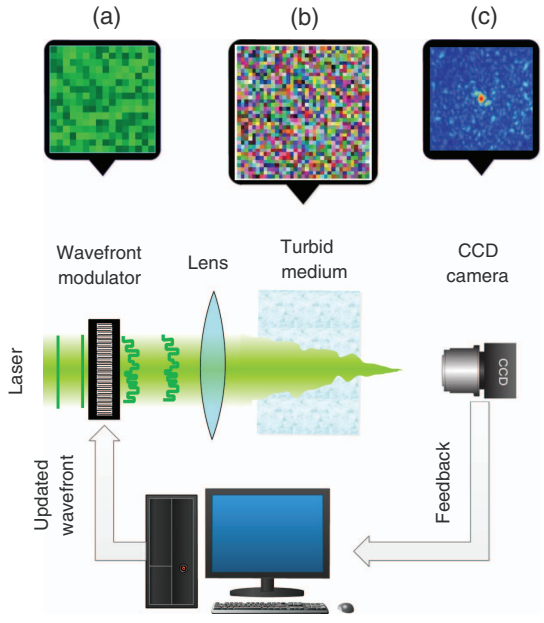


**Fig. 4.** Simulation setup: (a) represents the segments of a phase/amplitude map; (b) represents the TM of a turbid medium; and (c) is the transmitted light field at the CCD plane.

#### 1. Phase Optimization

In phase optimization, each input channel can be assigned a value between 0 and $2\pi$. This creates a very large search space. For instance, if the number of input channels (the phase modulator's pixels) is 1024, considering 10 quantization levels, the search space will have $1024^{10}$ solutions. Finding an optimum solution, in such a large search space, can be a very time-consuming task. Optimization algorithms reduce the size of the search space and save a significant amount of time in the search process.

In the SA optimization algorithm, the phase values of the input channels are perturbed at each iteration. We use two types of perturbations, namely, coarse perturbation and fine perturbation. Coarse perturbation is defined as an addition of a large multiple of the phase step to the current phase value. Fine perturbation is an addition of a small multiple. The algorithm begins with iterations of the coarse perturbation (loop) and then continues with iterations of the fine perturbation. In the coarse perturbation loop, the algorithm lets the system explore the entire search space, potentially escaping the local optimum in order to approach the global optimum. The fine perturbation loop, however, is designed to guide the search toward the global optimum.

Due to the large number of pixels in the SLM, they are grouped into segments, and the phase values of each segment are changed simultaneously. Applying a perturbation to each segment is equivalent to a negligible alteration in the wavefront that transmits through the SLM; the phase values assigned to a group of segments are, therefore, simultaneously changed in each step. By doing so, faster progress in the objective function is expected. The search will also be less sensitive to measurement noise and can more rapidly recover from disturbances [2].

The initial perturbation size is defined as the percentage of input channels ($N$) that are perturbed initially. A perturbation is then added to the phase of the randomly selected input channels. In the simulation, initially 50% of the segments are perturbed (initial perturbation size) for $\pi/16$ at each iteration during the coarse perturbation loop. In simulating noisy environments ($\geq 0.9\langle I_0\rangle$), the perturbation is changed to $\pi/8$. After going through a few coarse perturbation loops, the average acceptance rate of the new solutions generated in the loop decreases significantly and the search enters the fine perturbation loop. It has been shown that the performance of the SA algorithm is optimal when 30%–40% of the perturbations are accepted [50,62]. At the end of each fine perturbation loop, the temperature decreases and the fine perturbation size is adjusted by 10% of its current value (rate of change of perturbation size) to keep the acceptance rate in the optimal range.

Of note, the acceptance rate gradually decreases as the temperature drops. The optimization algorithm stops when the termination criteria are met—that can be the intensity of the focus or the number of iterations or the minimum temperature.

Another critical parameter in SA is the initial temperature. Temperature links the difference between the target electric field after perturbation ($E_2$) and that before perturbation ($E_1$) with the acceptance probability $P_{\text{acc}}$:

$$\Delta E = E_2 - E_1, P_{\text{acc}} = \exp\left(\frac{\Delta E}{T}\right) \Rightarrow T = \frac{\Delta E}{ln(P_{\text{acc}})}. \quad (7)$$

If the initial acceptance probability is too high, unnecessary time is spent at the beginning of the optimization. If it is too low, then the search might be trapped in a local optimum. In our study, we used a random TM, with a circular Gaussian distribution, zero mean, and a standard deviation of unity, to simulate the turbid medium [58–60]. According to Eq. (2), the value of electric field, $E$, is directly proportional to the values of the TM elements. On the other hand, according to Eq. (7), the ratio of $\Delta E$ to $T$ is important for acceptance probability. Therefore, the optimum value of initial temperature depends on the standard deviation of the TM. Empirically, we calculated the optimum value of the initial temperature to be equal to the standard deviation of the TM elements.

The two parameters $L$ and $\alpha$, i.e., the number of solutions generated in each perturbation loop and the cooling ratio, respectively, have similar impacts on the performance of the optimization algorithm. A steep temperature slope, which corresponds to small values of $\alpha$, approaches zero quickly, and, therefore, a large number of iterations should be performed at each temperature. However, if a gradual temperature slope is used, a smaller number of iterations is sufficient. According to [63,64], $\alpha$ is usually chosen between 0.85 and 0.99. The higher the $\alpha$, the longer the algorithm takes to reach the final temperature and the better the enhancement in noisy environments. In our study, $\alpha = 0.9$ was used in noise-free environments, and increased to 0.99 in very noisy environments. Depending on the execution time or the desired enhancement, $L$ will be assigned a value between $N/16$ (noise-free environments) and $N/6$ (in highly noisy environments) iterations at each perturbation loop.

In some studies, the number of iterations has been increased as the temperature drops [63,65]. By doing so, we observed no significant improvement in the final result.

#### 2. Amplitude Optimization

Amplitude optimization is a simpler optimization task than phase optimization. In amplitude optimization, each segment can be either "on" or "off". It has been shown that the ratio of the number of "on" segments to "off" segments in an optimal amplitude mask is 1 : 1 [3]. Therefore, the algorithm starts with a random binary map in which about half of the segments are "on" and half are "off". This ratio should be consistent throughout the optimization process. Initially, the algorithm toggles 5% of the input channels. The percentage of toggled channels is updated in a manner similar to that in the fine perturbation loop in the phase optimization algorithm (see Algorithm 1). Other parameters such as initial temperature, cooling ratio, perturbation loop length, and termination criteria are also adjusted similarly to how they are adjusted in phase optimization.

Reviewing the literature and performing several experiments, we have come up with a few tips to tune the optimization parameters for a more efficient implementation of the SA algorithm. As a general rule, one may say that the longer the execution time, the higher the enhancement; however, there are limitations. Increasing the initial and final temperatures may not be as effective as slowing down the cooling process, e.g., increasing the cooling ratio or the number of perturbations at each temperature; increasing the cooling ratio is a more efficient way to slow down the cooling process. We do not recommend that the algorithm spend a large amount of time at high temperatures (at which almost all perturbations are accepted); one way to solve this problem is to set a cutoff temperature or simply by starting the algorithm at a lower temperature. We observed a considerable variation in the obtained solutions with a long execution time. We also observed that the results obtained from one long run are more reliable than the average of results obtained from several shorter runs. A summary of how to tune the optimization parameters in the SA algorithm is given in Fig. 5.

## 3. RESULTS AND DISCUSSION

In this section, we present the results of the SA algorithm and compare its performance with a widely used optimization algorithm, the CS algorithm. We also compare the results of these algorithms in noisy environments. Finally, we briefly compare the SA algorithm with four other algorithms. In our simulations, a measurement is defined as the process of measuring

| Parameter | Explanation | Suggested value |
|---|---|---|
| Initial perturbation size | Percentage of the number of input channels ($N$) that are initially perturbed | Phase: 50% $N$<br>Binary: 5% $N$ |
| Perturbation | Amount of perturbation in phase optimization | Fine: $\pi/16$<br>Coarse: $\pi/8$ |
| Perturbation size change rate | Percentage by which the perturbation size is changed during the temperature loops | 10% current perturbation size |
| Initial temperature | Assuming that the standard deviation of transmission matrix is 1 | 1 |
| Cooling ratio ($\alpha$) | Temperature decrease rate ($T_{n+1} = \alpha T_n$) | Ideal: 0.9<br>Noisy: 0.99 |
| Perturbation loop length ($L$) | Number of iterations generated in a loop before the temperature drops | Ideal: $N/16$<br>Noisy: $N/6$ |

**Fig. 5.** Summary of optimization parameters in the SA algorithm.

the intensity of a specific output channel ($I_m$) when a phase mask or an amplitude mask is chosen based on Eq. (2). Gaussian noise with a standard deviation of $0.1\langle I_0\rangle$, $0.3\langle I_0\rangle$, $0.6\langle I_0\rangle$, or $0.9\langle I_0\rangle$ was added to each of these measurements. $0.3\langle I_0\rangle$ represents a normal experimental environment [2].

### A. Phase Optimization

In the CS algorithm, the phase of each segment is cycled between 0 and $2\pi$ to find the optimum phase for each segment. Assuming 10 phase samples are applied for each segment, $10N$ measurements are required to optimize a full phase map. To make a fair comparison, the results of the SA algorithm are also obtained after $10N$ measurements. Figure 6 compares the performance of the SA and CS algorithms under the same noise conditions and system sizes.

The CS algorithm demonstrates better performance compared with the SA algorithm in a noise-free environment. As the level of measurement noise increases, its performance drops dramatically. The CS algorithm fails to improve the enhancement beyond 10% of its maximum value in environments with a noise level larger than $0.9\langle I_0\rangle$ [49]. In contrast to CS, SA is more resilient to noise (see Fig. 6). CS initially converges slowly, but converges more rapidly toward the end of the algorithm.

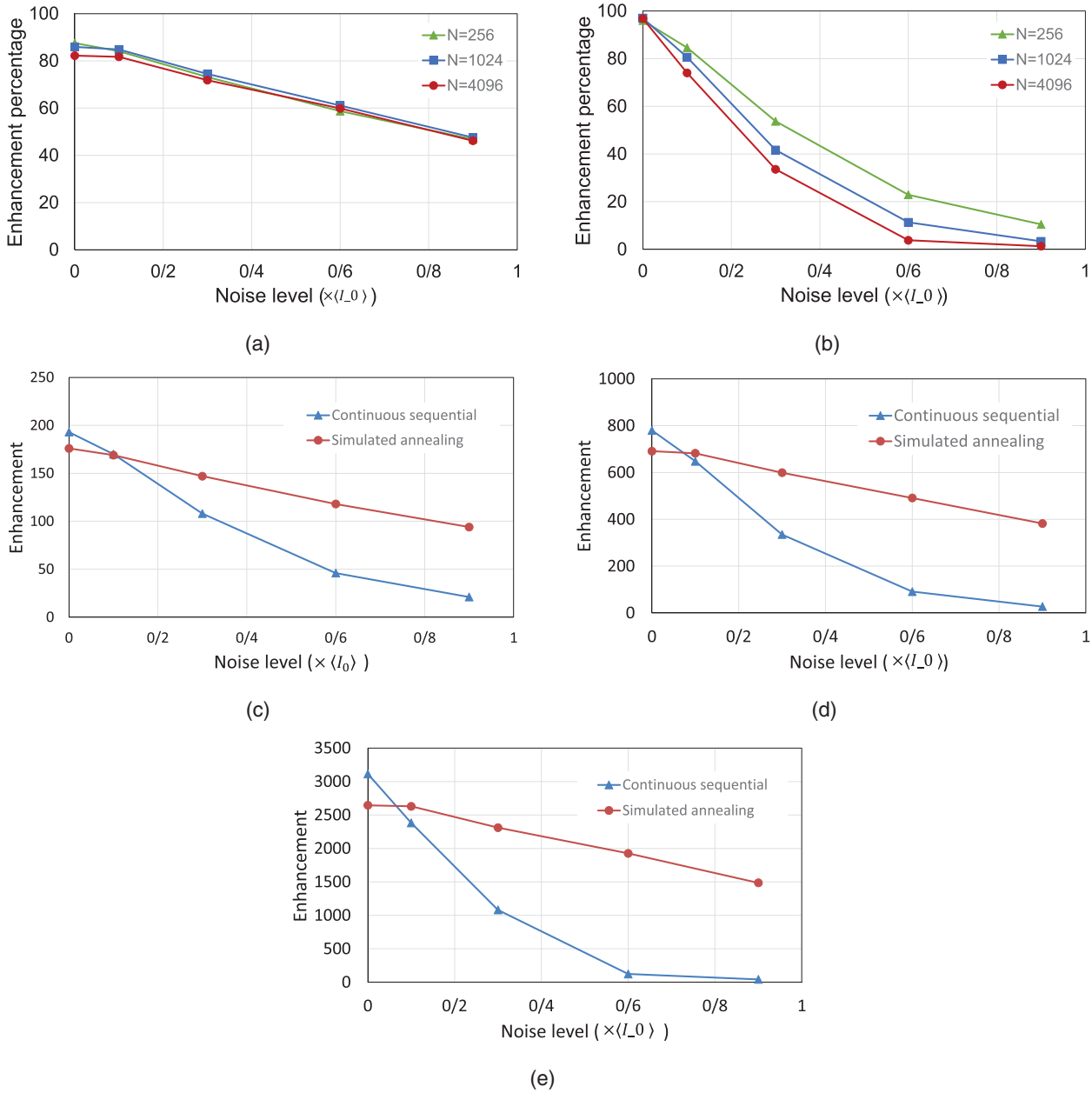


**Fig. 6.** Comparison between SA and CS algorithms with different system sizes at different measurement noise levels. (a) Enhancement versus different noise levels when the SA algorithm is used with a different number of input channels: 256, 1024, or 4096. (b) Enhancement versus different noise levels when the CS algorithm is used with a different number of input channels: 256, 1024, or 4096. (c)–(e) Enhancement versus noise level in CS and SA when the number of input channels is 256, 1024, or 4096. The data points are averaged over 20 runs.

SA converges fast in the beginning and slows down toward the end of the algorithm. Thus, SA can yield more acceptable results in a noisy environment in a relatively shorter time than that required by CS. The fast convergence time is particularly desirable for samples with a low persistence time. The performance of the SA algorithm does not change with increasing the size of the system. This is not the case with the CS algorithm, where performance degrades with increased system size.

### B. Amplitude Optimization

SA also offers promising performance improvement for DMD optimization, especially in noisy environments. Figure 7 presents the effect of the number of input channels on the execution time and enhancement. The enhancements of the algorithms are plotted versus the number of measurements. As demonstrated in Fig. 7, SA optimizes the system with different numbers of input channel robustly. Figure 8 shows the performance of the SA algorithm at different noise levels.

Wavefront shaping has an essential role in overcoming light scattering in turbid media. Several studies have investigated various optimization algorithms to find the optimum wavefront shape. Here, we comprehensively explored the SA algorithm, a heuristic algorithm for finding a global optimum of an objective function. SA is well suited for wavefront shaping because it can simultaneously optimize many input channels at once, thus reducing the effects of measurement noise better than linear solutions such as the CS algorithm and the TM estimation approach [46]. The SA algorithm reaches its optimum solution faster than the CS optimization algorithm. Thus, it is a prudent choice where a real-time algorithm is required—when working with samples with a low persistence time, for example.

In this study, we suggested a few tips as how to tune the optimization parameters. By introducing the perturbation loops and an adaptive perturbation system as explained in Section 2.E, we have improved the performance of the SA algorithm and its tolerance to measurement noise. The performance of SA in noisy environments can be improved further by using a PA as a pre-optimization step [2].

SA can also be tuned for a wide range of other applications by adjusting the cost function or the transmission matrices. For example, this approach can be extended to polarization-dependent [66], spectroscopic [67], and spatiotemporal

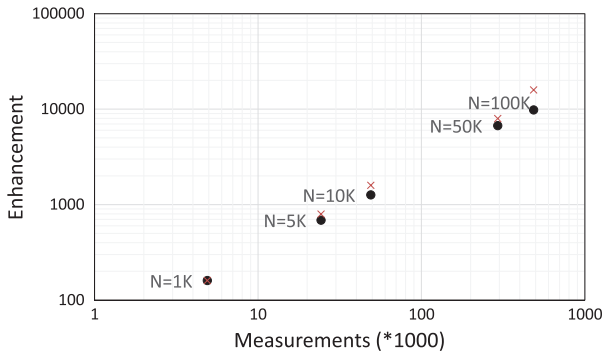


**Fig. 7.** Amplitude optimization using the SA algorithm. $N$ represents the number of input channels. Enhancements are close to the theoretical values (shown with red crosses) even in a large number of input channels. The data points are averaged over 20 runs.

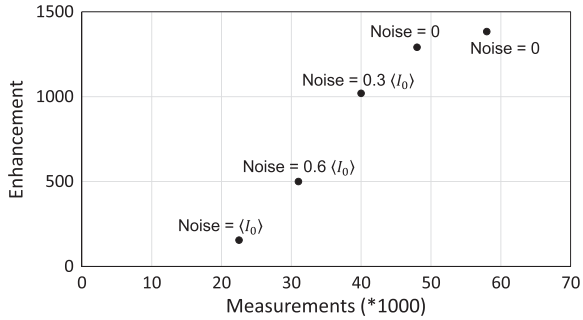


**Fig. 8.** Performance of the algorithm at different noise levels with $N = 10,000$. The data points are averaged over 20 runs.

wavefront shaping [68]. In each of these cases, the formalism of the transmission matrices would be different from the simple case that we have discussed in this work; this would, however, not change the overall performance of the algorithm, as the algorithm can be easily adjusted to work with any given cost function. It can also be easily tuned for multifocus transmission of beams by adding extra terms concerning the intensity of the new focuses to the cost function. Since SA is a parallel iterative optimization algorithm, it can be readily applied to measure the TM with wavefront shaping [69].

### C. Comparison with Other Algorithms

Since the first successful demonstration of wavefront shaping for controlled transmission, several other algorithms have been proposed for this purpose that have several advantages over the simple CS algorithm. A comprehensive comparison of all these algorithms in different noise conditions and for system sizes is out of scope of this work. Nevertheless, in this section, six optimization algorithms for wavefront shaping, including CS, PA, the TM estimation method, PSO, GA, and SA, are discussed and compared for a system with size $N = 256$ in noise-free conditions.

The PA algorithm has a fast initial enhancement increase. In each iteration of the PA, the segments are randomly divided over two equally sized partitions. Then the focus is maximized by cycling the phase of one partition with respect to the others from 0 to $2\pi$ (10 phases). This process is repeated until the termination condition, i.e., maximum number of measurements, is met [2].

The TM estimation method is a very flexible method and can be used to focus a beam on any desired target. In this method, for each input channel $n$, the algorithm iteratively sets the phase retardation to 0, $\pi/2$, $\pi$, and $3\pi/2$. Then the respective intensities in the $m$th output channel, $I_m^0$, $I_m^{\pi/2}$, $I_m^{\pi}$, and $I_m^{3\pi/2}$, are measured. It can be shown that the TM elements are then

$$t_{mn} = \frac{I_m^0 - I_m^{\pi}}{4} + i\frac{I_m^{\pi/2} - I_m^{3\pi/2}}{4} \tag{8}$$

up to a multiplicative factor, which is the same for all the elements of the matrix and can be eliminated [46]. Having the TM, one can easily set the phase mask to achieve a good focus. In this method, the TM can be estimated with $3N + 1$ measurements, which makes it a very fast method. However,

the performance of this method drops significantly in noisy conditions [70].

PSO is inspired by the social behavior of groups of animals and uses an efficient global information sharing mechanism. This algorithm begins by randomly generating a population of phase masks (particles). Each particle is then assigned an initial random velocity, which determines how the search space is explored. At the beginning, **pbest** stores the initial position (phase map) of each particle and the best position (with the highest focus intensity) of all particles is stored in **gbest**. Then the velocity and position of each particle are updated according to Eq. (10):

$$\mathbf{v_i^{k+1}} = w\mathbf{v_i^k} + c_1\mathbf{r_1^k}(\mathbf{pbest}_i^k - \mathbf{p_i^k}) + c_2\mathbf{r_2^k}(\mathbf{gbest^k} - \mathbf{p_i^k}), \quad (9)$$

$$\mathbf{p_i^{k+1}} = \mathbf{p_i^k} + \mathbf{v_i^k}, \quad (10)$$

where $\mathbf{v_i^k}$ and $\mathbf{p_i^k}$ are, respectively, the velocity and position vectors of the $i$th particle in the $k$th iteration and $w$ is the inertia weight. $c_1$ and $c_2$ are positive constants, which are called learning factors, and $\mathbf{r}_1$ and $\mathbf{r}_2$ are uniformly distributed random numbers between 0 and 1. Then, the new population is evaluated by measuring the fitness of each particle and comparing their fitness values with the **pbest** fitness value. If the new fitness is improved, then we update **pbest** with the current position of the particle. Afterwards, the best obtained fitness is compared with the population's overall previous best fitness (fitness of **gbest**). If a better fitness is obtained, we update **gbest** to the new best particle's phase map. This process continues until maximum number of iterations is reached [48,70].

The GA developed for focusing through turbid media begins by generating an initial population of phase masks. Each phase mask is created by selecting each input channel value from a uniform pseudorandom distribution of phase values between 0 and $2\pi$. First a population of phase masks is identified, and then the fitness value (focus intensity) of each mask is measured. The fitness function is used to rank the population of masks; masks with the highest intensity receive a higher ranking. To improve the phase masks, the algorithm uses an iterative breeding and mutation operation. Using a random binary breeding template, $B$, two randomly selected parent masks (ma and pa) are chosen for breeding from the population. The probability of selection for breeding is determined by the ranking of the phase masks. Using $B$, the input channels of the parent masks are combined, creating a new offspring. The offspring mask is then mutated by changing the phase of a small percentage of input channels at random: Offspring $= ma \cdot B + pa \cdot (1 - B)$. This new mask is again mutated by randomly changing the phase of a small percentage of input channels [49].

Figure 9 presents the results of implementing the following algorithms: CS and SA are implemented as explained in Section 2.E. The PA and TM estimation methods do not have any specific free parameters. The PSO was implemented with a population size of 50. The algorithm ran for 50 iterations. The constriction coefficient method was used to set the values of $w = 0.73$ and $c_1 = c_2 = 1.5$ [71]. The phases were chosen to be between 0 and $2\pi$. The velocities were limited to a range of $[-2\pi/10, 2\pi/10]$ to avoid very large steps. The population size for the GA algorithm was also set to 50 and the crossover rate was set to 0.5. The parents were chosen with the tournament method [49]. Mutation was applied on 10% of the population in each generation. The phase of 0.1 of the input channels (mutation rate) of the selected population was mutated by a value of $4\pi/10$. In order to prevent the algorithm from mutating too many optimized phase modes, the mutation rate was decreased from the initial value of 0.1 to a value of 0.002 as the algorithm reaches the end of optimization. Note that these simulations were run for the ideal, noise-free environment. The performance of CS and TM, which seem to be better here, would degrade considerably in noisy environments [70].

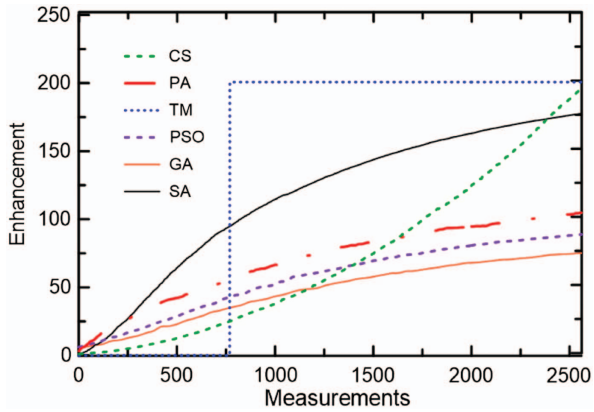


**Fig. 9.** Illustration of the performance of the CS, PA, TM method, PSO, GA, and SA for $N = 256$, comparing the enhancement of the focus with the number of measurements. The curves are averaged over 20 runs [70].

## 4. CONCLUSION

SA is an efficient and effective algorithm to find the optimum wavefront shape for focusing light through a turbid medium. We implemented the SA algorithm for optimization of phase and amplitude modulators with different system sizes (in phase optimization, $N = 256$, 1024, 4096; in amplitude optimization, $N = 1$ K, 5 K, 10 K, 50 K, 100 K) at different measurement noise levels (0, $0.1\langle I_0\rangle$, $0.3\langle I_0\rangle$, $0.6\langle I_0\rangle$, $0.9\langle I_0\rangle$). The major optimization parameters, including temperature, cooling ratio, perturbation loop length, and perturbation size, were tuned based on our suggested tips. Key findings in this study were as follows: in a noise-free environment, the CS algorithm outperforms SA, whereas in noisy environments, SA performs significantly better than CS. As opposed to CS, in SA the ratio of experimental enhancement to theoretical enhancement at different system sizes is almost the same. Optimization using the SA algorithm has an initial rapid enhancement growth, which makes SA an appropriate algorithm in applications that need fast convergence.

This study suggests that SA is a promising and efficient algorithm for wavefront optimization of phase or amplitude modulators. Comparing the performance of the SA and CS algorithms with those of other established optimization algorithms for wavefront shaping is in progress and planned for the future.

**Acknowledgment.** This research has been supported by Hamamatsu Photonics and Wayne State startup. Special thanks go to Chris Haig and Daniela Maldonado from Hamamatsu Photonics for their fruitful discussions.

## REFERENCES


1. A. Mosk, A. Lagendijk, G. Lerosey, and M. Fink, "Controlling waves in space and time for imaging and focusing in complex media," Nat. Photonics **6**, 283–292 (2012).
2. I. Vellekoop and A. Mosk, "Phase control algorithms for focusing light through turbid media," Opt. Commun. **281**, 3071–3080 (2008).
3. D. Akbulut, T. J. Huisman, E. G. van Putten, W. L. Vos, and A. P. Mosk, "Focusing light through random photonic media by binary amplitude modulation," Opt. Express **19**, 4017–4029 (2011).
4. R. Fiolka, K. Si, and M. Cui, "Complex wavefront corrections for deep tissue focusing using low coherence backscattered light," Opt. Express **20**, 16532–16543 (2012).
5. J. Jang, J. Lim, H. Yu, H. Choi, J. Ha, J. H. Park, W. Y. Oh, W. Jang, S. Lee, and Y. Park, "Complex wavefront shaping for optimal depth-selective focusing in optical coherence tomography," Opt. Express **21**, 2890–2902 (2013).
6. H. Yu, J. Jang, J. Lim, J.-H. Park, W. Jang, J.-Y. Kim, and Y. Park, "Depth-enhanced 2-D optical coherence tomography using complex wavefront shaping," Opt. Express **22**, 7514–7523 (2014).
7. I. N. Papadopoulos, S. Farahi, C. Moser, and D. Psaltis, "High-resolution, lensless endoscope based on digital scanning through a multimode optical fiber," Biomed. Opt. Express **4**, 260–270 (2013).
8. N. Ji, D. E. Milkie, and E. Betzig, "Adaptive optics via pupil segmentation for high resolution imaging in biological tissues," Nat. Methods **7**, 141–147 (2010).
9. J. Y. Tang, R. N. Germain, and M. Cui, "Superpenetration optical microscopy by iterative multiphoton adaptive compensation technique," Proc. Natl. Acad. Sci. USA **109**, 8434–8439 (2012).
10. X. D. Tao, Z. Dean, C. Chien, O. Azucena, D. Bodington, and J. Kubby, "Shack–Hartmann wavefront sensing using interferometric focusing of light onto guidestars," Opt. Express **21**, 31282–31292 (2013).
11. J. Park, W. Sun, and M. Cui, "High-resolution *in vivo* imaging of mouse brain through the intact skull," Proc. Natl. Acad. Sci. USA **112**, 9236–9241 (2015).
12. K. Si, R. Fiolka, and M. Cui, "Breaking the spatial resolution barrier via iterative sound–light interaction in deep tissue microscopy," Sci. Rep. **2**, 748 (2012).
13. B. Judkewitz, Y. M. Wang, R. Horstmeyer, A. Mathy, and C. H. Yang, "Speckle-scale focusing in the diffusive regime with time reversal of variance-encoded light (TROVE)," Nat. Photonics **7**, 300–305 (2013).
14. T. Chaigne, O. Katz, A. C. Boccara, M. Fink, E. Bossy, and S. Gigan, "Controlling light in scattering media non-invasively using the photoacoustic transmission matrix," Nat. Photonics **8**, 58–64 (2014).
15. H. Yu, J. Park, K. Lee, J. Yoon, K. Kim, S. Lee, and Y. Park, "Recent advances in wavefront shaping techniques for biomedical applications," Curr. Appl. Phys. **15**, 632–641 (2015).
16. M. Leonetti and C. Lopez, "Active subnanometer spectral control of a random laser," Appl. Phys. Lett. **102**, 071105 (2013).
17. M. Leonetti, C. Conti, and C. Lopez, "Random laser tailored by directional stimulated emission," Phys. Rev. A **85**, 043841 (2012).
18. N. Bachelard, S. Gigan, X. Noblin, and P. Sebbah, "Adaptive pumping for spectral control of random lasers," Nature **10**, 426–431 (2014).
19. N. Bachelard, J. Andreasen, S. Gigan, and P. Sebbah, "Taming random lasers through active spatial control of the pump," Phys. Rev. Lett. **109**, 033903 (2012).
20. E. Small, O. Katz, Y. Guan, and Y. Silberberg, "Spectral control of broadband light through random media by wavefront shaping," Opt. Lett. **37**, 3429–3431 (2012).
21. J. H. Park, C. Park, H. Yu, Y. H. Cho, and Y. Park, "Dynamic active wave plate using random nanoparticles," Opt. Express **20**, 17010–17016 (2012).
22. H. P. Paudel, C. Stockbridge, J. Mertz, and T. Bifano, "Focusing polychromatic light through strongly scattering media," Opt. Express **21**, 17299–17308 (2013).
23. F. van Beijnum, E. G. van Putten, A. Lagendijk, and A. P. Mosk, "Frequency bandwidth of light focused through turbid media," Opt. Lett. **36**, 373–375 (2011).
24. D. J. McCabe, A. Tajalli, D. R. Austin, P. Bondareff, I. A. Walmsley, S. Gigan, and B. Chatel, "Spatio-temporal focusing of an ultrafast pulse through a multiply scattering medium," Nat. Commun. **2**, 447 (2011).
25. O. Katz, E. Small, Y. Bromberg, and Y. Silberberg, "Focusing and compression of ultrashort pulses through scattering media," Nat. Photonics **5**, 372–377 (2011).
26. J. H. Park, C. Park, H. Yu, Y. H. Cho, and Y. Park, "Active spectral filtering through turbid media," Opt. Lett. **37**, 3261–3263 (2012).
27. Y. Guan, O. Katz, E. Small, J. Zhou, and Y. Silberberg, "Polarization control of multiply scattered light through random media by wavefront shaping," Opt. Lett. **37**, 4663–4665 (2012).
28. I. M. Vellekoop, A. Lagendijk, and A. P. Mosk, "Exploiting disorder for perfect focusing," Nat. Photonics **4**, 320–322 (2010).
29. E. G. van Putten, D. Akbulut, J. Bertolotti, W. L. Vos, A. Lagendijk, and A. P. Mosk, "Scattering lens resolves sub-100 nm structures with visible light," Phys. Rev. Lett. **106**, 193905 (2011).
30. I. M. Vellekoop, M. Cui, and C. Yang, "Digital optical phase conjugation of fluorescence in turbid tissue," Appl. Phys. Lett. **101**, 081108 (2012).
31. S. R. Huisman, T. J. Huisman, S. A. Goorden, A. P. Mosk, and P. W. H. Pinkse, "Programming balanced optical beam splitters in white paint," Opt. Express **22**, 8320–8332 (2014).
32. F. J. Rodriguez, C. Yao, J. Bravo-Abad, and J. Martorell, "Spatial control of second-harmonic light from a disordered structure," Proc. SPIE **8425**, 84251D (2012).
33. C. Yao, F. Rodriguez, and J. Martorell, "Controlling the diffused nonlinear light generated in random materials," Opt. Lett. **37**, 1676–1678 (2012).
34. T. Huisman, S. Huisman, A. P. Mosk, and P. Pinkse, "Controlling single-photon Fock-state propagation through opaque scattering media," Appl. Phys. B **116**, 603–607 (2014).
35. S. F. Liew, S. M. Popoff, S. W. Sheehan, A. Goetschy, C. A. Schmuttenmaer, A. D. Stone, and H. Cao, "Coherent control of photocurrent in a disordered photovoltaic system," arXiv:1507.07438 (2015).
36. D. Wang, E. Zhou, J. Brake, H. Ruan, M. Jang, and C. Yang, "Focusing through dynamic tissue with millisecond digital optical phase conjugation," Optica **2**, 728–735 (2015).
37. Y. Ren, G. Xie, H. Huang, N. Ahmed, Y. Yan, L. Li, C. Bao, M. P. J. Lavery, M. Tur, M. A. Neifeld, R. W. Boyd, J. H. Shapiro, and A. E. Willner, "Adaptive-optics-based simultaneous pre- and post-turbulence compensation of multiple orbital-angular-momentum beams in a bidirectional freespace optical link," Optica **1**, 376–382 (2014).
38. D. Conkey and R. Piestun, "Color image projection through a strongly scattering wall," Opt. Express **20**, 27312–27318 (2012).
39. X. Yang, N. Chia-Lung, H. Y. Pu, and D. Psaltis, "Three-dimensional scanning microscopy through thin turbid media," Opt. Express **20**, 2500–2506 (2012).
40. T. Strudley, R. Bruck, B. Mills, and O. L. Muskens, "An ultrafast reconfigurable nanophotonic switch using wavefront shaping of light in a nonlinear nanomaterial," Light Sci. Appl. **3**, e207 (2014).
41. R. Burton, A. Klimas, C. Ambrosi, J. Tomek, A. Corbett, E. Entcheva, and G. Bub, "Optical control of excitation waves in cardiac tissue," Nat. Photonics **9**, 813–816 (2015).
42. B. Anderson, R. Gunawidjaja, and H. Eilers, "Effect of experimental parameters on optimal reflection of light from opaque media," Phys. Rev. A **93**, 013813 (2016).
43. B. Anderson, R. Gunawidjaja, and H. Eilers, "Effect of experimental parameters on optimal transmission of light through opaque media," Phys. Rev. A **90**, 053826 (2014).
44. B. Anderson, R. Gunawidjaja, and H. Eilers, "Initial tamper tests of novel tamper-indicating optical physical unclonable functions," Appl. Opt. **56**, 2863–2872 (2017).
45. I. Freund, "Looking through walls and around corners," Physica A **168**, 49–65 (1990).

46. S. Popoff, G. Lerosey, R. Carminati, M. Fink, A. Boccara, and S. Gigan, "Measuring the transmission matrix in optics: an approach to the study and control of light propagation in disordered media," Phys. Rev. Lett. **104**, 100601 (2010).
47. D. Dudley, W. Duncan, and J. Slaughter, "Emerging digital micromirror device (DMD) applications," Proc. SPIE **4985**, 1–12 (2003).
48. H. Huang, Z. Chen, C. Sun, J. Liu, and J. Pu, "Light focusing through scattering media by particle swarm optimization," Chin. Phys. Lett. **32**, 104202 (2015).
49. D. Conkey, A. Brown, A. Caravaca-Aguirre, and R. Piestun, "Genetic algorithm optimization for focusing through turbid media in noisy environments," Opt. Express **20**, 4840–4849 (2012).
50. N. Metropolis, A. Rosenbluth, M. Rosenbluth, A. Teller, and E. Teller, "Equation of state calculations by fast computing machines," J. Chem. Phys. **21**, 1087–1092 (1953).
51. N. Yoshikawa and T. Yatagai, "Phase optimization of a kinoform by simulated annealing," Appl. Opt. **33**, 863–868 (1994).
52. S. Zommer, E. Ribak, S. Lipson, and J. Adler, "Simulated annealing in ocular adaptive optics," Opt. Lett. **31**, 939–941 (2006).
53. M. R. Nasiri-Avanaki, S. Hojjatoleslami, H. Paun, S. Tuohy, A. Meadway, G. Dobre, and A. Podoleanu, "Optical coherence tomography system optimization using simulated annealing algorithm," in *Mathematical Methods and Applied Computing* (2009), p. 669.
54. M. Avanaki, A. Bradu, and A. Podoleanu, "Optimization of excitation of fiber Fabry–Perot tunable filters used in swept lasers using a phase-correction method," Appl. Opt. **56**, 3378–3382 (2017).
55. M. Avanaki, A. Bradu, I. Trifanov, A. Ribeiro, A. Hojjatoleslami, and A. Podoleanu, "Algorithm for excitation optimization of Fabry–Perot filters used in swept sources," IEEE Photon. Technol. Lett. **25**, 472–475 (2013).
56. M. Avanaki, Y. Long, M. A. Paun, S. A. Hojjatoleslami, and A. Gh. Podoleanu, "Fast algorithm for blind optimization of optical systems," Int. J. Electron. **101**, 1179–1189 (2013).
57. Z. Fayyaz, F. Salimi, N. Mohammadian, A. Fatima, M. R. R. Tabar, and M. R. N. Avanaki, "Wavefront shaping using simulated annealing algorithm for focusing light through turbid media," Proc. SPIE **10494**, 104946M (2018).
58. J. Goodman, *Statistical Optics* (Wiley, 2000).
59. N. Garcia and A. Genack, "Crossover to strong intensity correlation for microwave radiation in random media," Phys. Rev. Lett. **63**, 1678–1681 (1989).
60. M. Webster, T. Gerke, A. Weiner, and K. Webb, "Spectral and temporal speckle field measurements of a random medium," Opt. Lett. **29**, 1491–1493 (2004).
61. C. Beenakker, "Random-matrix theory of quantum transport," Rev. Mod. Phys. **69**, 731–808 (1997).
62. A. Mashaghi, P. Partovi-Azar, T. Jadidi, M. Anvari, S. Jand, N. Nafari, M. R. R. Tabar, P. Maass, H. Bakker, and M. Bonn, "Enhanced autoionization of water at phospholipid interfaces," J. Phys. Chem. C **117**, 510–514 (2012).
63. S. Kirkpatrik, C. D. Gelatt, Jr., and M. P. Vecchi, "Optimization by simulated annealing," Science **220**, 671–680 (1983).
64. K. Du and M. Swamy, *Search and Optimization by Metaheuristics* (2016).
65. H. Sanvicente Sánchez and J. Frausto-Solis, "A method to establish the cooling scheme in simulated annealing like algorithms," in *Computational Science and Its Applications—ICCSA*, Lecture Notes in Computer Science (2004), Vol. **3045**, pp. 755–763.
66. J. Park, C. Park, H. Yu, Y. Cho, and Y. Park, "Dynamic active wave plate using random nanoparticles," Opt. Express **20**, 17010–17016 (2012).
67. J. Park, C. Park, H. Yu, Y. Cho, and Y. Park, "Active spectral filtering through turbid media," Opt. Lett. **37**, 3261–3263 (2012).
68. J. Aulbach, B. Gjonaj, P. Johnson, A. Mosk, and A. Lagendijk, "Control of light transmission through opaque scattering media in space and time," Phys. Rev. Lett. **106**, 103901 (2011).
69. J. Yoon, K. Lee, J. Park, and Y. Park, "Measuring optical transmission matrices by wavefront shaping," Opt. Express **23**, 10158–10167 (2015).
70. Z. Fayyaz, N. Mohammadian, and M. R. N. Avanaki, "Comparative assessment of five algorithms to control an SLM for focusing coherent light through scattering media," Proc. SPIE **10494**, 104946I (2018).
71. R. C. Eberhart and J. Kennedy, "A new optimizer using particle swarm theory," in *Sixth International Symposium on Micromachine and Human Science* (1995), pp. 39–43.